metals

MDPI

Article

Morphological Characteristics of W/Cu Composite Nanoparticles with Complex Phase Structure Synthesized via Reactive Radio Frequency (RF) Thermal Plasma

Chulwoong Han [1,2], Song-Yi Kim [1], Soobin Kim [2] and Ji-Woon Lee [3,*]

[1] Korea Institute of Industrial Technology (KITECH), Incheon 21999, Republic of Korea; hcholw@kitech.re.kr (C.H.); commence@kitech.re.kr (S.-Y.K.)
[2] Department of Materials Science and Engineering, Inha University, Incheon 22212, Republic of Korea; binz000@inha.edu
[3] Division of Advanced Materials Engineering, Kongju National University, Cheonan 31080, Republic of Korea
* Correspondence: jwl@kongju.ac.kr

Abstract: The W/Cu binary system is characterized by its mutual insolubility and excellent wettability, making W/Cu composite materials ideal for managing thermal and electrical properties in electronic components. To optimize material properties, control over the microstructure is crucial, and nanocomposites with uniform dispersion offer significant advantages. In this study, W/Cu composite nanoparticles were synthesized by feeding a blended feedstock of tungsten trioxide (WO_3) micro-powder and cupric oxide (CuO) micro-powder into a reactive radio frequency (RF) argon–hydrogen thermal plasma system. Cu-coated W nanocomposite particles were obtained through the vaporization, reduction, and condensation processes. The resulting nanocomposite particles were composed of body-centered cubic (BCC) α-W, A15 β-W, and face-centered cubic (FCC) Cu phases, with a chemical composition closely matching theoretical calculations. The phase evolution and morphological changes of the synthesized particles were analyzed as a function of heat treatment temperatures up to 1000 °C in a reducing atmosphere. Up to 600 °C, the phase composition and morphology remained stable. At 800 °C, localized diffusion and coalescence of Cu led to the formation of particulate Cu, and a significant phase transformation from metastable β-W to α-W was observed. Additionally, extensive Cu segregation due to long-range diffusion resulted in distinct Cu-rich and Cu-depleted regions. In these regions, notable sintering of W particles and the complete disappearance of β-W occurred. The results showed that the temperature-dependent redistribution of Cu plays a crucial role in the phase transformation of W and the morphology of W/Cu composite particles.

Keywords: W/Cu composite nanoparticle; heat treatment; Cu redistribution; morphology

Citation: Han, C.; Kim, S.-Y.; Kim, S.; Lee, J.-W. Morphological Characteristics of W/Cu Composite Nanoparticles with Complex Phase Structure Synthesized via Reactive Radio Frequency (RF) Thermal Plasma. *Metals* **2024**, *14*, 1070. https://doi.org/10.3390/met14091070

Academic Editor: Imre Bakonyi

Received: 16 August 2024
Revised: 5 September 2024
Accepted: 9 September 2024
Published: 18 September 2024

1. Introduction

Nanoparticle synthesis is broadly classified into solid-, liquid-, and vapor-based processes, depending on the primary phase responsible for nanoparticle generation [1,2]. Among these, RF thermal plasma synthesis falls under the vapor-based process [3]. The use of electrodeless thermal plasma, generated through inductively coupled radio frequency (RF) thermal plasma, helps to prevent contamination [4,5]. In this method, the extended residence time of particles in flight allows for enhanced energy transfer from the thermal plasma due to the reduced momentum of the plasma itself [6,7]. Axial feedstock injection ensures that particles in flight follow similar trajectories, thereby improving the uniformity of the reaction. Furthermore, the introduction of quenching gas into the vapor phase creates a sharp temperature gradient, which is advantageous for the condensation of vapor species, thus facilitating effective nanoparticle formation.

In addition to its advantages, the broad material selectivity offered by RF thermal plasma is particularly appealing for nanoparticle synthesis [6–9]. Typically, solid feedstock

micro-powder is vaporized, and nanoparticles nucleate and grow from the resulting supersaturated vapor [9,10]. However, RF thermal plasma has traditionally been used for the synthesis of monolithic nanoparticles due to challenges in achieving uniform chemical composition in multi-component systems at the particle level. Nevertheless, in cases like the W/Cu binary system, where composite nanoparticles are synthesized, the uniform distribution of constituent phases becomes more critical than the precise chemical composition [11]. The W/Cu binary system is unique due to the complete mutual insolubility of W and Cu and their differing thermophysical properties. By adjusting the chemical composition and microstructure, a wide range of thermal and electrical properties can be achieved. Traditionally, W/Cu composite materials are fabricated through either Cu infiltration or liquid phase sintering. In liquid phase sintering, the infiltration of molten Cu into the W skeleton leads to densification, which largely depends on the wettability of Cu on W [12,13]. Extensive research has focused on improving the homogeneous dispersion of W and Cu phases [14]. To achieve this, nanoparticles should be synthesized and then sintered.

The conventional method for preparing W/Cu nanocomposites involves dynamic milling of WO_3 and CuO, followed by reduction of the oxide components and subsequent sintering. In this study, W/Cu nanocomposite particles were synthesized using a reactive RF thermal plasma process as a new method to fabricate W/Cu nanocomposites. The morphological characteristics of the as-synthesized nanoparticles were analyzed, and their morphological evolution was observed in relation to the heat treatment temperature.

2. Materials and Methods

Cu-coated W composite nanoparticles were synthesized by feeding a blended feedstock of WO_3 (>99.99%, LTS Inc., Herndon, VA, USA) and CuO (>99.99%, LTS Inc., USA) with irregular shapes into a reactive RF thermal plasma system. A detailed schematic image of the system is shown in Figure 1. The structure and internal constitution of the system can be found elsewhere in detail [15]. Process parameters are summarized in Table 1. Hydrogen gas was chosen as a reducing agent, and it was fed through sheath gas for the protection of the generated plasma. WO_3 micro-powder with an average particle size (D_{50}) of 47.7 μm and CuO micro-powder with an average particle size (D_{50}) of 6.8 μm were wet-blended using a turbulent mixer in a reaction of 4:1 (WO_3:CuO) of which molar ratio was 0.56:0.44 (WO_3:CuO). The selected composition is an optimal condition considering densification and high electrical conductivity. Complete densification is difficult under a composition of 20 wt.% Cu or less because the contact angle of Cu with respect to W is large [16].

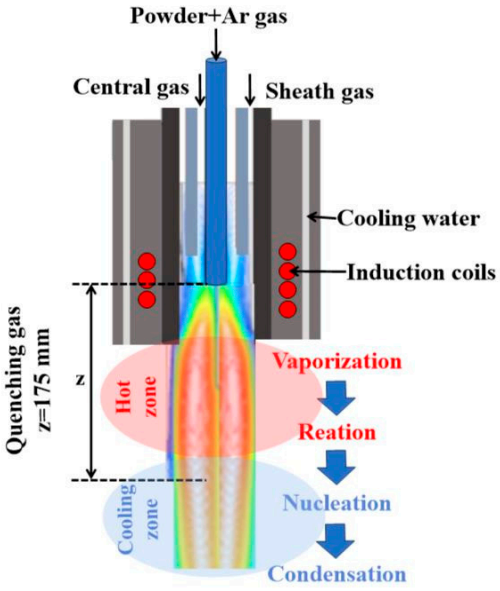

Figure 1. Schematic illustration of a reactive RF thermal plasma system.

Table 1. RF thermal plasma process parameters.

Feedstock		Plasma Power	Plasma Gas (slpm)					
Weight of Blended Feedstock	**Feed Rate**	**-**	**Pressure**	**Central Gas**	**Carrier Gas**	**Sheath Gas**	**Sheath Gas**	**Quench Gas**
80 g WO_3, 20 g CuO	5 g·min^{-1}	28 kW	14.7 psia	Ar 15	Ar 5	Ar 60	H_2 10	Ar 100

In order to evaluate thermal stability of the synthesized powder, nanoparticles were heated to 200, 400, 600, 800, and 1000 °C at the heating rate of 10 °C·min^{-1} in a resistance furnace under reducing environment (H_2). As the temperature reached a target temperature, particles were then subsequently cooled in the furnace and remained. During the heat treatment, the hydrogen gas flow rate was 5 slpm.

Synthesized nanoparticles were obtained, and the overall chemical composition of particles was measured by elemental mapping using energy dispersive spectroscopy (EDS) via an FEI Quanta 200F field-emission scanning electron microscope (FE-SEM) (FEI company, Hillsboro, OR, USA) after the reactive RF thermal plasma process. The overall Cu weight fraction was measured as 18 wt.% and showed good consistency with theoretically calculated values in the blended feedstock. The phase composition was analyzed using a Bruker D8 Discover X-ray diffractometer (XRD) (Bruker Corporation, Billerica, MA, USA).

The morphology and chemical compositions of both as-synthesized particles and the heat-treated particles were investigated using scanning transmission electron microscopy (STEM) and EDS via a FEI TECNAI G2 TEM.

3. Results

Figure 2 shows the morphologies of the W/Cu composite nanoparticles synthesized using a reactive RF thermal plasma process. The high energy density and reactivity of the argon–hydrogen thermal plasma enable the complete vaporization, reduction, and subsequent condensation of a blended feedstock composed of WO_3 and CuO micro-powders into W/Cu metallic nanoparticles. The cuboid and spherical W/Cu nanoparticles are well observed in the TEM images (Figure 2) with average particle sizes of 26.2 nm. To assess the distribution of Cu, STEM-EDS analysis was performed, providing elemental maps. The elemental maps for both W and Cu indicate that Cu is uniformly distributed on the W surface, which is further confirmed by the distribution of Cu content, as measured by elemental mapping analysis and depicted in Figure 2d. Although some particles exhibit partial segregation of Cu, Cu is consistently present on all particles. Consequently, these synthesized particles are identified as Cu-coated W composite particles.

During the RF thermal plasma synthesis of nanoparticles, in-flight particles undergo a thermal cycle of heating and cooling within a limited residence time, making the vaporization of the solid feedstock a critical step in nanoparticle generation. The high energy density of the thermal plasma allows the in-flight particles to be heated by convective heat transfer. The phase evolution of these particles depends on the balance between the energy transferred from the thermal plasma and the energy stored within the particles. When the transferred energy exceeds the energy required for phase transformation, the particles undergo heating, melting, and vaporization. Under specific thermal plasma operating conditions, the required energy and vaporization efficiency is influenced by the physical and thermophysical properties of the feedstock materials. In this context, WO_3 and CuO are particularly favorable for vaporization, as their boiling points (1700 °C for WO_3 and 2000 °C for CuO) are significantly lower than those of W (5555 °C) and Cu (2562 °C).

Beyond vaporization, the chemical reactivity of the thermal plasma must also be considered to achieve the reduction of oxide feedstock to metallic material. In RF thermal plasma, hydrogen serves as an effective reducing agent for WO_3 and CuO, while also enhancing the plasma's thermal conductivity. Furthermore, hydrogen molecules dissociate into hydrogen atoms within the thermal plasma. According to the conventional nucleation

model of reduction [17], the rate-determining step in the reaction kinetics is the adsorption and dissociation of hydrogen molecules. Therefore, the presence of atomic hydrogen is beneficial for the reduction of oxide species. Nanoparticles are then formed from the reduced vapor cloud through condensation processes. The introduction of quenching gas into the vapor cloud creates a sharp temperature gradient, causing the vapor to become supersaturated and promoting homogeneous nucleation at critical supersaturation levels. The formation of liquid particulate matter depends on the level of supersaturation, which is influenced by vapor pressure and temperature. Initially, W condenses, followed by Cu during cooling. This difference in critical supersaturation temperatures between W and Cu contributes to the formation of Cu-coated W nanoparticles. In this study, it appears that the heterogeneous condensation of Cu vapor on W particles or enhanced diffusion of Cu on W particles after collision plays a significant role.

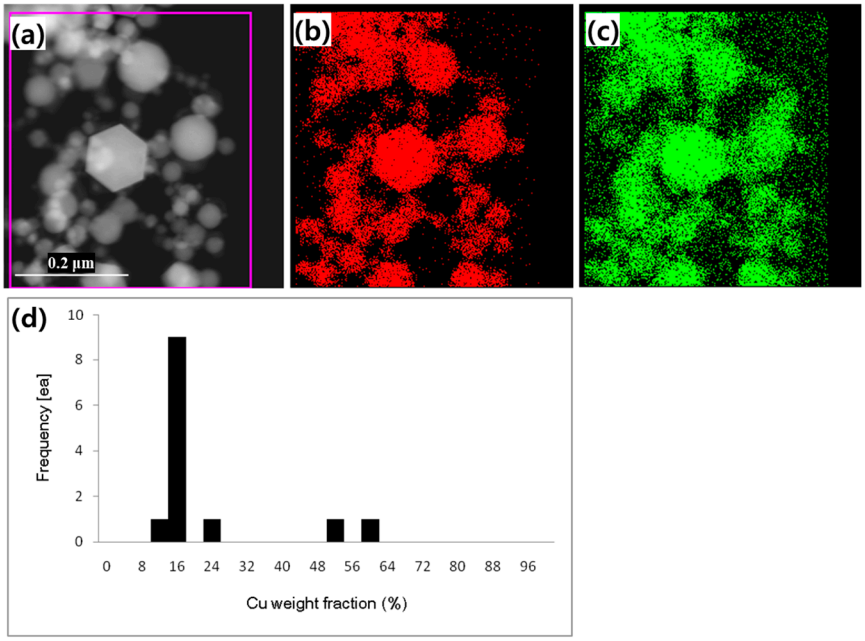

Figure 2. (**a**) STEM image showing morphology, elemental maps of (**b**) W and (**c**) Cu, and (**d**) histogram of Cu weight fraction in W/Cu composite nanoparticles synthesized via RF thermal plasma process.

Figure 3 shows the changes in the phase composition of the W/Cu composite nanoparticles with respect to the heat treatment temperature. The as-synthesized W/Cu nanoparticles consist of both stable α-W and metastable β-W (W_3O). As the heat treatment temperature increases, a noticeable phase transformation from β-W into α-W occurs. The relative phase fraction of β-W, denoted as X_β, is quantified using the following relationship:

$$X_\beta = \frac{A_{\beta(210)}}{A_{\alpha(110)} + A_{\beta(210)}} \quad (1)$$

where $A_{\alpha(110)}$ and $A_{\beta(210)}$ are the peak areas of the (110) peak of α-W and the (210) peak of β-W, respectively. The peak areas, A_α and A_β, were determined from the XRD diffraction pattern, and peaks were deconvoluted. β-W remains stable after heat treatment at 600 °C, but a significant portion of β-W transforms into α-W at 800 °C. Finally, the complete transformation from β-W to α-W is observed at 1000 °C.

Morphological changes were examined after heat treatment of the as-synthesized Cu-coated W composite nanoparticles. Figure 4 shows the morphologies of the W/Cu composite nanoparticles heat-treated at 800 °C. Significant changes in both morphology and Cu distribution were observed only after heat treatment at 800 °C. On a macroscopic level, the particles treated at 800 °C retain a morphology similar to that of the as-synthesized

particles. However, the distribution of Cu and W becomes more distinct, as seen in the elemental maps for W and Cu. Unlike the as-synthesized particles, Cu-rich particles can be separated from W-rich ones, as further confirmed by elemental quantification at the particle level (Figure 4d). The observed morphology and distribution of Cu indicate that localized Cu particulates form due to the short-distance diffusion and coalescence of Cu on the W surface. These Cu segregates typically manifest as particulate Cu or faceted Cu. Faceted Cu is characterized by its ability to bridge W particles with its faceted surface. At 800 °C, it is more common to see localized clusters where W particles are attached to particulate Cu. Notably, W particles are often isolated from each other by intermediate Cu segregates.

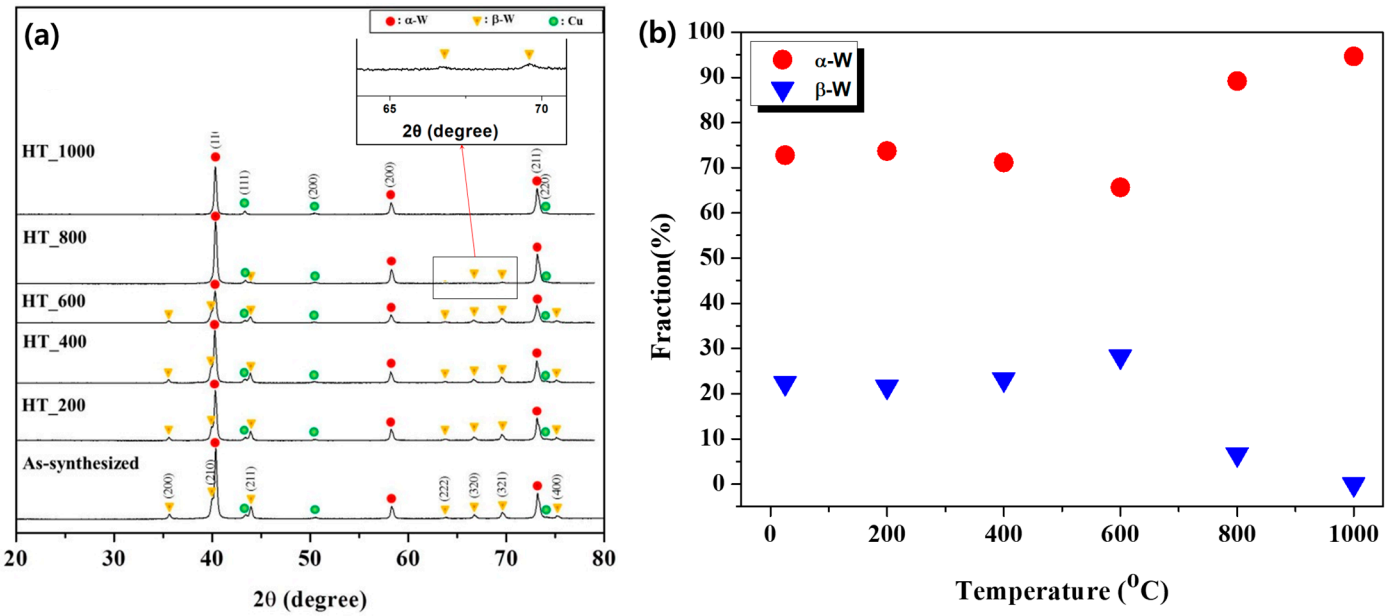

Figure 3. (**a**) X-ray diffraction pattern showing phase evolution and (**b**) phase fractions of α-W and β-W with respect to the heat treatment temperature in W/Cu composite nanoparticles synthesized via the RF thermal plasma process.

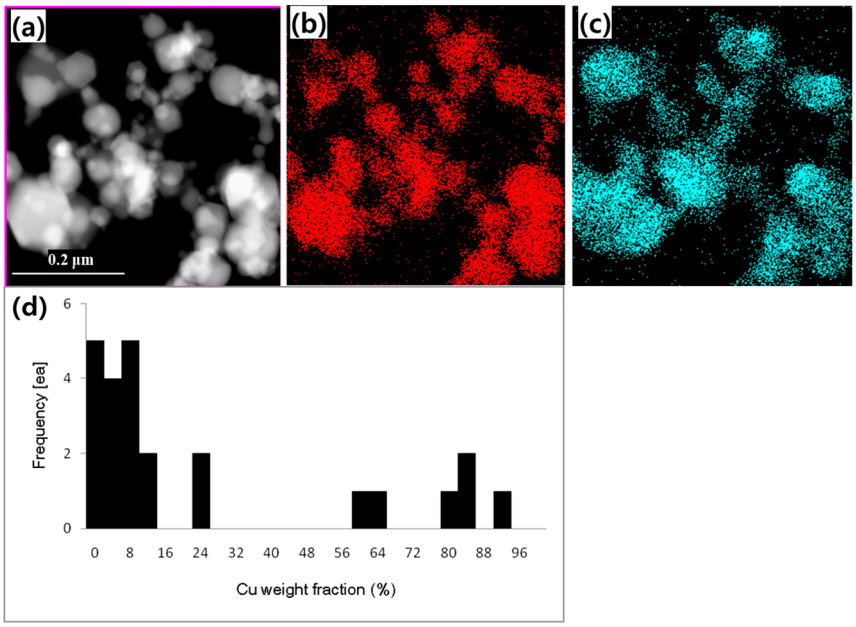

Figure 4. (**a**) STEM image showing morphology, elemental maps of (**b**) W, (**c**) Cu, and (**d**) histogram of Cu weight fraction in W/Cu composite nanoparticles heat-treated at 800 °C.

After heat treatment at 1000 °C, the W/Cu composite nanoparticles exhibit a significantly different morphology compared to the as-synthesized particles. The high temperature leads to intense Cu diffusion and redistribution, resulting in noticeable Cu segregation and particle sintering, as shown in Figure 5. There is a clear phase separation into pure W and pure Cu particles, with a high probability of occurrence, as illustrated in Figure 5d. A cross-sectional sample of the Cu-segregated region was prepared using the focused ion beam (FIB) for further investigation. Figure 6 presents the FIB sample, revealing a dense Cu-segregated region (marked as [A]) and a porous Cu-depleted region (marked as [B]). Discrete Cu segregation is confirmed by the variation in Cu weight fraction between the Cu-segregated and Cu-depleted regions, as depicted in Figure 6. From a morphological perspective, the Cu-segregated region is characterized by W particles embedded within Cu, as shown in the STEM image. Meanwhile, in the Cu-depleted region, W particles exhibit hard agglomeration and growth. In summary, the particles heat-treated at 1000 °C show severe Cu segregation, which markedly increases W contiguity.

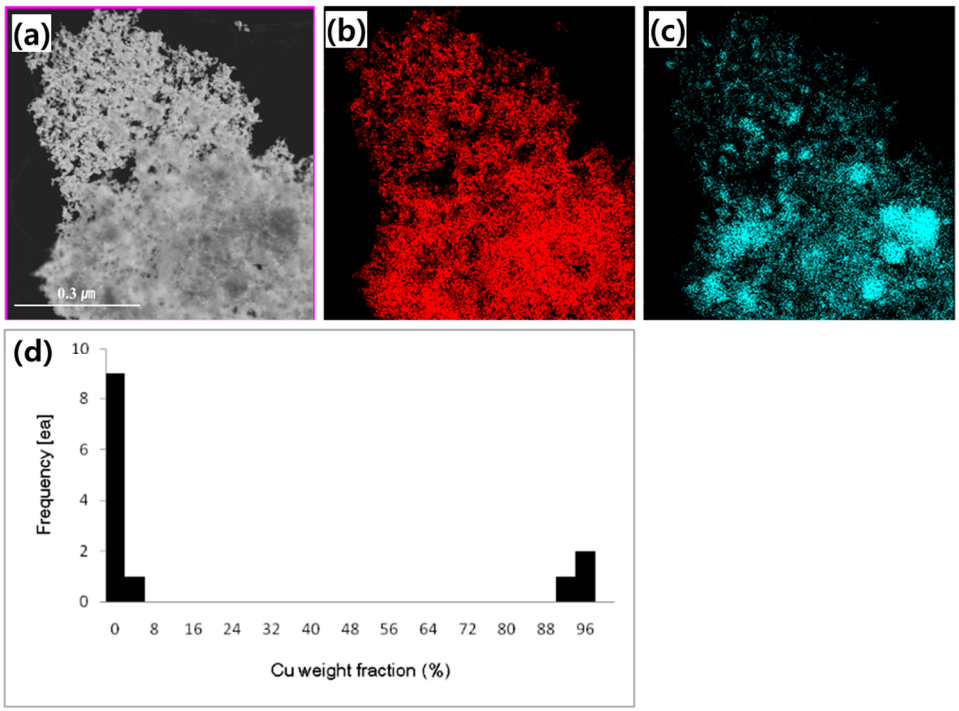

Figure 5. (**a**) STEM image showing morphology, elemental maps of (**b**) W, (**c**) Cu, and (**d**) histogram of Cu weight fraction in W/Cu composite nanoparticles heat-treated at 1000 °C.

Microstructure showed that Cu-coated W nanocomposite particles were effectively synthesized using reactive RF thermal plasma synthesis, and the morphological changes of the particles were investigated at various heat treatment temperatures in a reducing environment. The composite powder remains stable up to 800 °C. The primary factor influencing morphological evolution is the redistribution of Cu. As the temperature increases, the diffusion distance and the extent of Cu segregation also increase, along with the contiguity between W nanoparticles. Although the particles of W grow, the pressure and low temperature of liquid Cu and the low probability of contact with small and large particles of W hinder particle growth, so there is little change in particle size due to heat treatment. These morphological changes are further discussed from the perspective of both Cu redistribution and W clustering in the discussion section.

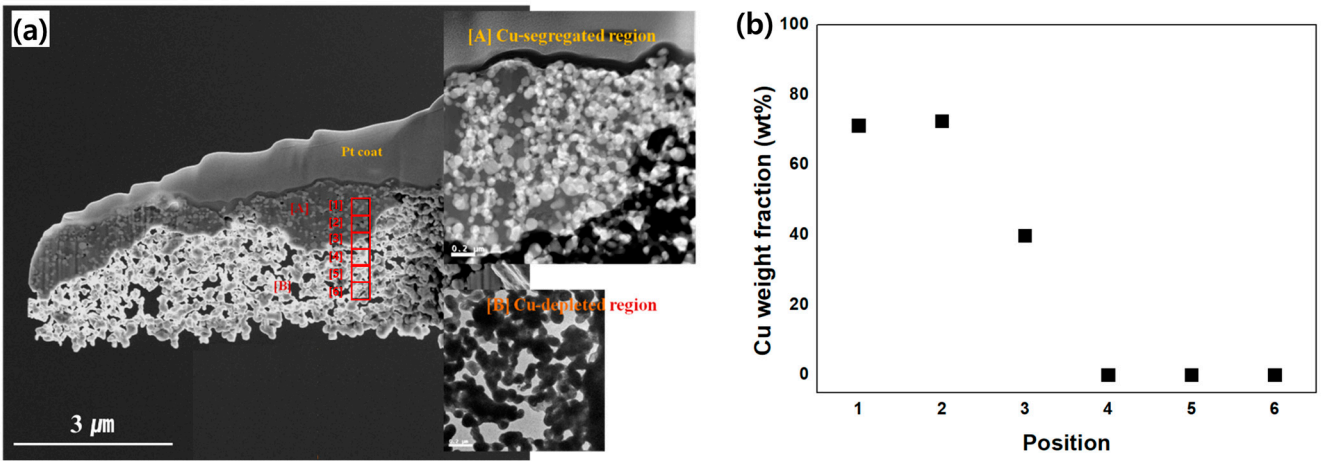

Figure 6. (**a**) Cross-sectional morphology of Cu segregated region in FIBed sample heat-treated at 1000 °C showing severe segregation of Cu particles and W particle growth. EDS results at the position from 1 to 6 in (**a**) are represented in (**b**).

4. Discussion

The thermal and electrical properties of W/Cu composite materials are heavily influenced by their microstructures, including several parameters such as phase fraction, constituent phase size, distribution, and porosity [18]. Research in powder metallurgy generally concludes that achieving a fully dense composite with a uniform microstructure is optimal for thermal and electrical management. However, most studies focus on the morphological changes caused by the mass transport of molten Cu during liquid phase sintering. The mass transport behavior of nanoparticles differs significantly from that of micro-sized particles due to size effects. In this study, using Cu-coated W nanocomposite powder, the Cu diffusion rate is increased due to the extended surface area, and W nanoparticles tend to sinter together spontaneously at a reduced homologous temperature below 0.3 T_m [19]. Therefore, solid-state morphological changes are crucial for determining the final microstructure of W/Cu composites. In this context, these morphological changes are considered from the perspective of temperature-dependent Cu redistribution and the morphological evolution of W clusters in W/Cu composite nanoparticles.

4.1. Temperature-Dependent Cu Redistribution

The W/Cu binary system has been extensively studied in the context of thin-film technology, particularly Cu interconnection. Cu exhibits strong bonding with the W substrate, and a monolayer of Cu has high thermal stability [20]. However, Cu bonds less strongly with underlying Cu layers. When Cu-coated W nanocomposites are heated, the diffusion and coalescence of Cu atoms occur, reducing surface energy. As a result, significant Cu diffusion on W follows a surface self-diffusion mode due to both the mutual insolubility of W and Cu and the strong bond between the Cu monolayer and the underlying W particle. The surface diffusivity of Cu is largely dependent on the temperature and environment. According to a previous study [19], Cu surface self-diffusion becomes significant above 660 °C in a reducing environment, and the diffusivity at 1000 °C is an order of magnitude higher than that at 800 °C. Additionally, Cu faceting on a sinusoidal surface topology occurs at below 910 °C, consistent with the present study.

The elemental distribution of W and Cu in the as-synthesized composite particles is shown in Figure 7a, where Cu is uniformly distributed on W particles. Up to 600 °C, no significant morphological changes are observed in the W/Cu composite particles due to the sluggish diffusivity of Cu. However, at 800 °C, Cu redistribution results in the exposure of W particles and localized Cu enrichment, with Cu surrounded by W particles, as shown in Figure 7b. This may be due to the short diffusion distance and the faceting behavior of Cu on the highly curved W particle surfaces. At 1000 °C, the diffusion distance of Cu is much

longer than at 800 °C, leading to the clear development of Cu-segregated and Cu-depleted regions, as shown in Figure 7c. This significant Cu redistribution is driven by temperature-dependent surface self-diffusivity to reduce surface energy and local melting Cu particles may be responsible for the segregation. The variation in Cu content, as measured by STEM-EDS at the particle level, aligns with the elemental maps across different heat treatment temperatures. In addition, the element distribution of the sample made by the RF plasma process in this study is relatively more uniform compared to the nanoparticles made by the ball milling process [21]. Since stainless steel containers and balls are used during the ball milling process, the milling powder is likely to be contaminated by Fe, Ni, Cr, etc., which act as active sintering additives.

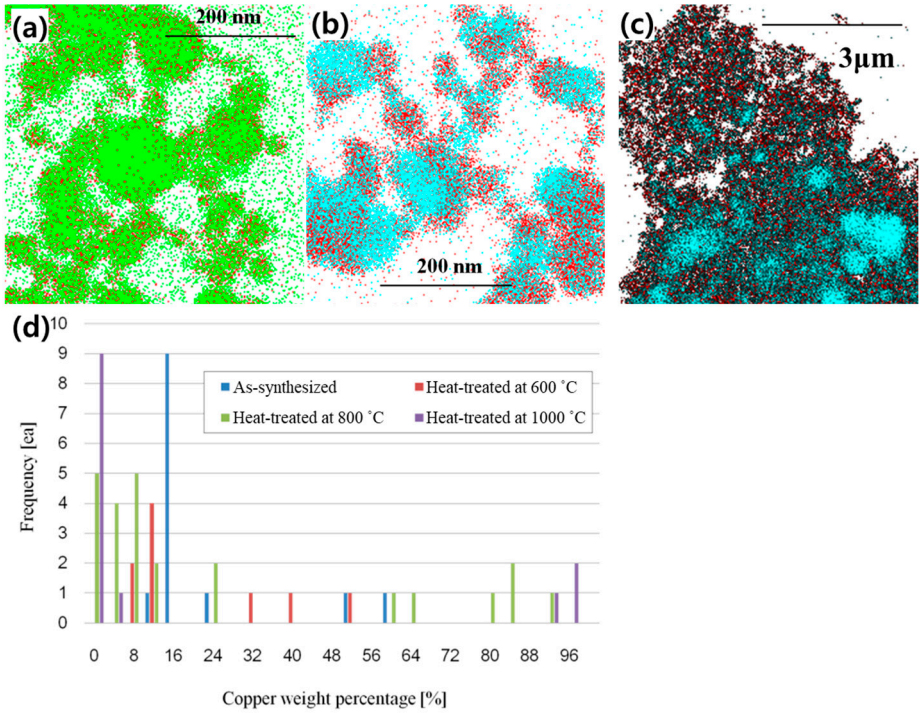

Figure 7. Elemental maps showing Cu distribution in (**a**) as-synthesized nanoparticles, (**b**) heat-treated nanoparticles at 800 °C, (**c**) heat-treated nanoparticles at 1000 °C, and (**d**) a histogram of the Cu weight fraction in W/Cu composite nanoparticles with respect to the heat treatment temperature. Red dots represent W and other colors represent Cu in elemental maps.

Furthermore, Cu redistribution appears to be related to the phase transformation of W. As mentioned earlier, the transformation from β-W to α-W is prominent at 800 °C and is completed at 1000 °C. β-W is often observed in the physical vapor deposition of W thin films [22] and is known as a metastable phase with an A15 structure, stabilized by interstitial impurities [23]. Typically, phase transformation to stable α-W occurs at around 650 °C and is likely related to oxygen diffusion. In fact, β-W can remain stable up to 950 °C in nanorods with sluggish oxygen diffusivity [23]. In this study, the β-to-α transformation shows high thermal stability, which may be influenced by the degree of Cu redistribution. Indeed, the β-to-α transformation of W corresponds with the Cu redistribution and particle composition observed in Figure 7. W particles remain enveloped by Cu up to 600 °C, and at 800 °C, a significant portion of W particles become exposed due to Cu diffusion, although Cu-coated W particles are still present, as shown by elemental quantification. The enhanced Cu diffusion and phase separation lead to the complete disappearance of β-W at 1000 °C. Consequently, the presence of Cu on the surface of β-W may retard the phase transformation by inhibiting oxygen diffusion into β-W.

4.2. W Nanoparticle Cluster

In this study, Cu redistribution by diffusion becomes evident above 800 °C, significantly impacting the contiguity and sintering of W nanoparticles. This is demonstrated by the morphological changes in W nanoparticles observed at different heat treatment temperatures and positions, as shown in Figure 8. While the composite particle heated at 800 °C appears to be sintered compared to the as-synthesized particle, this is primarily due to localized Cu redistribution and faceting effects, with fine nanoparticles remaining stable. The limited Cu diffusion at 800 °C leads to the formation of localized Cu and W clusters, where W nanoparticles surround the Cu. In this case, the W particles remain isolated, as the temperature is insufficient for the vigorous sintering of the W nanoparticles. However, significant particle sintering is observed in the composite powder heat-treated at 1000 °C. Figure 8c shows a Cu-depleted region where the Cu content was less than 2 wt.% according to the areal quantification. It is suggested that the severe segregation of Cu, due to enhanced diffusivity, increases the contiguity of W particles, causing the W nanoparticles to spontaneously coalesce at 1000 °C. This results in the formation of a W skeleton framework composed of partially sintered W clusters. Moreover, the morphological differences in W between Cu-segregated and Cu-depleted regions highlight the effect of Cu on W sintering (Figure 8d). In the Cu-segregated regions, W particles, isolated by Cu, maintain their fine particle size and particulate morphology. Consequently, Cu prevents W particles from sintering by isolating them, with no mutual solubility between the two.

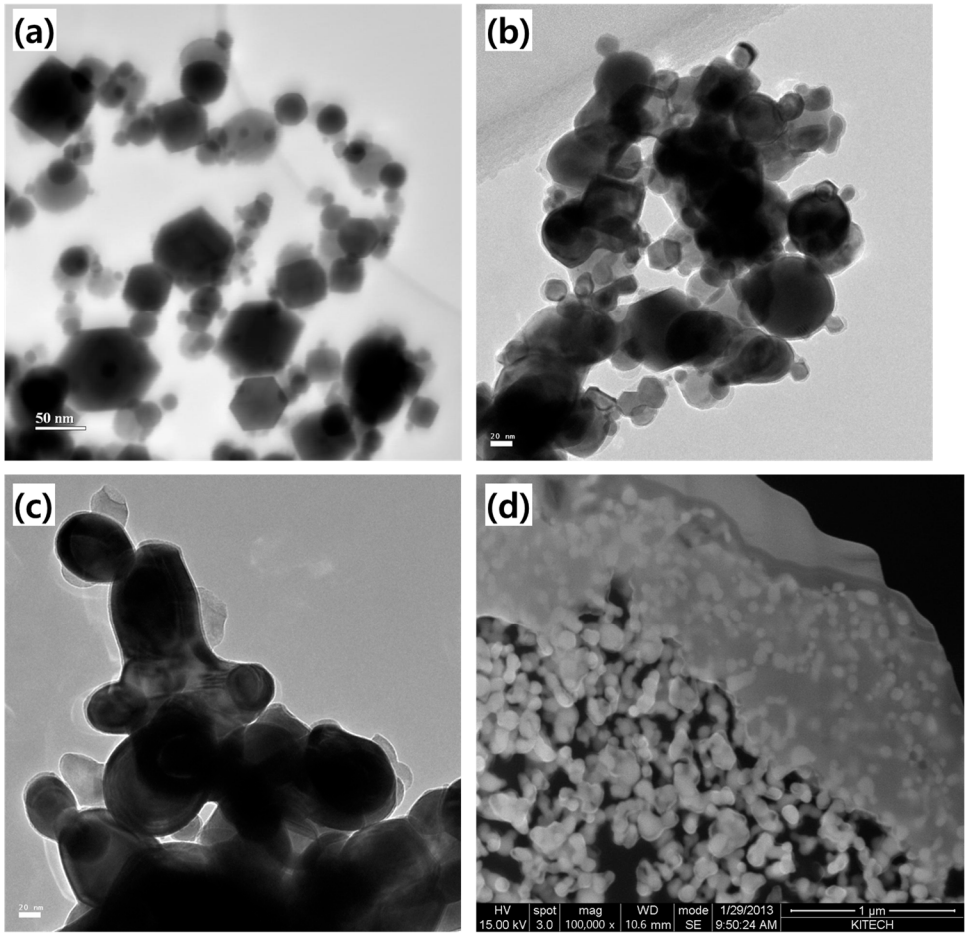

Figure 8. TEM images of (**a**) as-synthesized composite particles, (**b**) heat-treated composite particles at 800 °C, (**c**) heat-treated composite particles at 1000 °C, and F Elemental maps showing Cu distribution in (**a**) as-synthesized nanoparticles, (**b**) heat-treated nanoparticles at 800 °C, (**c**) heat-treated nanoparticles at 1000 °C, and (**d**) FE-SEM image of heat-treated nanoparticles at 1000 °C represented for comparison of W particle morphology at Cu-segregated region and Cu-depleted region.

The synthesis and sintering mechanisms of Cu-coated W composite nanoparticles are schematically summarized in Figure 9. Cu-coated W composite nanoparticles are synthesized via reactive RF thermal plasma process. As the heat treatment temperature increases within the solid state, the degree of Cu diffusion and redistribution intensifies. Due to the temperature-dependent diffusivity of Cu, severe segregation occurs through localized Cu redistribution. This redistribution also alters the contiguity of W particles. As the heat treatment temperature rises, W contiguity increases, leading to enhanced sintering between contacting W nanoparticles. The resulting sintered W clusters can serve as building blocks for subsequent liquid phase sintering. The sintering of the W clusters progresses before Cu migrates back toward the network of sintered W clusters. Therefore, the solid-state morphological changes driven by Cu redistribution are considered critical steps in determining the microstructure of W/Cu composite materials.

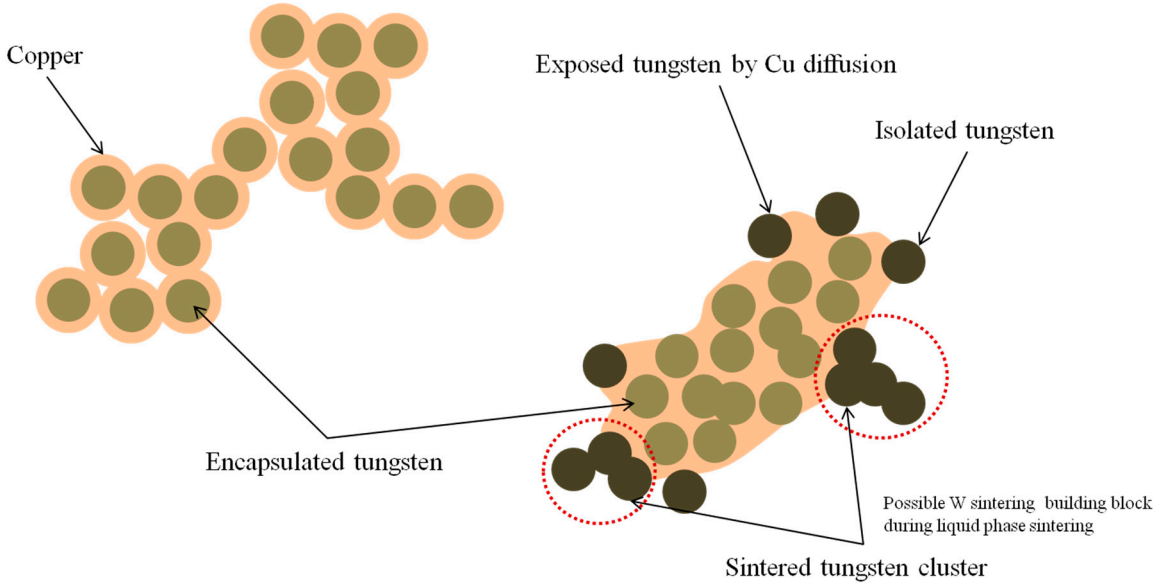

Figure 9. Schematic illustration of mechanism for synthesis and sintering of Cu-coated W composite nanoparticles.

5. Conclusions

W/Cu composite nanoparticles were successfully synthesized by introducing a blended feedstock of tungsten trioxide and cupric oxide micro-powder via an argon–hydrogen reactive RF thermal plasma process. Based on the observed changes in particle size and phase composition, it is concluded that the WO_3 and CuO particles undergo a vaporization–reduction–condensation process within the reactive RF thermal plasma. The as-synthesized W/Cu composite nanoparticle features a W core coated with Cu. Chemical composition analysis at the particle level consistently detected the presence of Cu. After heat treatment in a reducing environment, Cu redistribution leads to the localized formation of particulate Cu, with W particles remaining isolated from each other due to the presence of intermediate Cu after heating at 800 °C. However, extensive Cu segregation through long-range diffusion creates distinct Cu-rich and Cu-depleted regions. In the Cu-depleted areas, the contact and sintering of W particles are enhanced, resulting in the formation of W clusters. Conversely, W particles embedded in Cu-segregated regions maintain a particulate morphology, with sintering being suppressed due to the presence of Cu, which has no solubility with W. In conventional liquid phase sintering, particles are heated above the melting point of Cu, passing through a solid-state phase. This study suggests that solid-state morphological changes, particularly the formation of W clusters, may be a critical step in determining the microstructure of W/Cu composite materials.

Author Contributions: Conceptualization, C.H.; methodology, C.H.; investigation, C.H., S.-Y.K. and S.K.; data curation, C.H., S.-Y.K. and S.K.; writing—original draft preparation, C.H.; writing—review and editing, J.-W.L.; funding acquisition, C.H. and J.-W.L. All authors have read and agreed to the published version of the manuscript.

Funding: This research was supported by the research grant of the Kongju National University in 2022 and partly supported by "Regional Innovation Strategy (RIS)" through the National Research Foundation of Korea (NRF) funded by the Ministry of Education (MOE) (2021RIS-004).

Data Availability Statement: The original contributions presented in the study are included in the article, further inquiries can be directed to the corresponding author.

Conflicts of Interest: The authors declare no conflicts of interest.

References

1. Kumari, S.; Raturi, S.; Kulshrestha, S.; Chauhan, K.; Dhingra, S.; András, K.; Thu, K.; Khargotra, R.; Singh, T. A comprehensive review on various techniques used for synthesizing nanoparticles. *J. Mater. Res. Technol.* **2023**, *27*, 1739–1763. [CrossRef]
2. Harish, V.; Ansari, M.M.; Tewari, D.; Yadav, M.G.A.B.; García-Betancourt, M.; Abdel-Haleem, F.M.; Bechelany, M.; Barhoum, A. Nanoparticle and Nanostructure Synthesis and Controlled Growth Methods. *Nanomaterials* **2023**, *12*, 3226. [CrossRef]
3. Na, H.; Lee, W.; Choi, H. Characteristics of Ni–W bimetallic nanoparticle via reactive RF thermal plasma synthesis. *Int. J. Refract. Metals Hard Mater.* **2015**, *53*, 17–22. [CrossRef]
4. Herdrich, G.; Auweter-Kurtz, M. Inductively heated plasma sources for technical applications. *Vacuum* **2006**, *80*, 1138–1143. [CrossRef]
5. Bai, Y.; Zhao, L.; Qu, Y.M.; Fu, Q.Q.; Wang, Y.; Liu, K.; Tang, J.J.; Li, B.Q.; Han, Z.H. Particle in-flight behavior and its influence on the microstructure and properties of supersonic-atmospheric-plasma-sprayed nanostructured thermal barrier coatings. *J. Alloys Compd.* **2015**, *644*, 873–882. [CrossRef]
6. Heimann, R.B. The Nature of Plasma Spraying. *Coatings* **2023**, *13*, 622. [CrossRef]
7. Yaochun, Y.; Hossain, M.M.; Watanabe, T. Numerical and experimental investigation on the in-flight melting behaviour of granulated powders in induction thermal plasmas. *Plasma Sources Sci. Technol.* **2009**, *11*, 71–77. [CrossRef]
8. Han, C.; Na, H.; Choi, H. Vapor phase condensation synthesis of refractory metal and oxide nano-particles. In Proceedings of the European Congress and Exhibition on Powder Metallurgy. European PM Conference Proceedings, Gothenburg, Sweden, 15–18 September 2013; pp. 1–7.
9. Piao, Y.; Burns, A.; Kim, J.; Wiesner, U.; Hyeon, T. Designed fabrication of silica-based nanostructured particle systems for nanomedicine applications. *Adv. Funct. Mater.* **2008**, *18*, 3745–3758. [CrossRef]
10. Kim, K.; Kim, B.; Choi, H. Size and morphology manipulation of nickel nanoparticle in inductively coupled thermal plasma synthesis. *J. Alloys Compd.* **2016**, *658*, 824–831. [CrossRef]
11. Björketun, M.E.; Bondarenko, A.S.; Abrams, B.L.; Chorkendorf, I.; Rossmeisl, J. Screening of electrocatalytic materials for hydrogen evolution. *Phys. Chem. Chem. Phys.* **2010**, *12*, 10536–10541. [CrossRef]
12. Ibrahim, H.; Aziz, A.; Rahmat, A. Enhanced liquid-phase sintering of W–Cu composites by liquid infiltration. *Int. J. Refract. Metals Hard Mater.* **2014**, *43*, 222–226. [CrossRef]
13. Ibrahim, H.; Aziz, A.; Rahmat, A.; Mohammed, K.S. Comparison of liquid phase sintering and Cu-melt infiltration methods to consolidate 80W-Cu composite using Nickel as sintering activator. *Appl. Mech. Mater.* **2013**, *372*, 34–40.
14. Hou, C.; Song, X.; Tang, F.; Li, Y.; Cao, L.; Wang, J.; Nie, Z. W–Cu composites with submicron- and nanostructures: Progress and challenges. *NPG Asia Mater.* **2019**, *11*, 74–93. [CrossRef]
15. Cho, S.; Han, C.; Choi, H.; Kim, H.; Jin, S.; Han, J. Synthesis and consolidation behavior of Al/AlN composite powders by reactive RF thermal plasma spraying. *Powder Technol.* **2016**, *287*, 395–402. [CrossRef]
16. Kingery, W.D. Densification during Sintering in the Presence of a Liquid Phase. I. Theory. *J. Appl. Phys.* **1959**, *30*, 301–306. [CrossRef]
17. Ding, S.; Duan, J.; Chen, S. Recent advances of metal suboxide catalysts for carbon-neutral energy applications. *EcoEnergy* **2024**, *2*, 45–82. [CrossRef]
18. Chen, P.; Luo, G.; Shen, Q.; Li, M.; Zhang, L. Thermal and electrical properties of W–Cu composite produced by activated sintering. *Mater. Des.* **2013**, *46*, 101–105. [CrossRef]
19. Nazrul-Islam, S.M.K.; Mayank, P.; Ouyang, Y.; Chen, J.; Sagotra, A.K.; Li, M.; Cortie, M.B.; Mole, R.; Cazorla, C.; Yu, D.; et al. Copper diffusion rates and hopping pathways in superionic Cu2Se. *Acta Mater.* **2021**, *215*, 117026–117035. [CrossRef]
20. Hsu, W.; Yang, S.; Lin, Y.; Chang, H.; Chiang, C.; Hsieh, W.; Tu, K.; Chiu, W.; Chen, C. Measurement of Thermal Stress by X-ray Nano-Diffraction in (111)-Oriented Nanotwinned Cu Bumps for Cu/SiO_2 Hybrid Joints. *Nanomaterials* **2023**, *13*, 2448. [CrossRef]
21. Park, H.R.; Ryu, S.S. Characteristics of WO_3-CuO Powder Mixture Prepared by High-Energy Ball Milling in a Bead Mill for the Synthesis of W-Cu Nanocomposite Powder. *J. Korean Powder Metall. Inst.* **2017**, *24*, 406–413. [CrossRef]

22. Velicu, I.; Tiron, V.; Porosnicu, C.; Burducea, I.; Lupu, N.; Stoian, G.; Popa, G.; Munteanu, D. Enhanced properties of tungsten thin films deposited with a novel HiPIMS approach. *Appl. Surf. Sci.* **2017**, *424*, 397–406. [CrossRef]
23. Sluiter, M.H.F. Interstitials in tetrahedrally close-packed phases: C, N, O, and F in β-tungsten from first principles. *Phys. Rev. B* **2009**, *80*, 220102. [CrossRef]